HALF-MODEL TESTING AND SIDEWALL EFFECTS

M. R. Soltani, A. Mamaghani, A. Bakhshalipour
Sharif University of Technology, Tehran, Iran

Keywords: *half-model, suction, pressure, lift, wake*

Abstract

An extensive experimental test to study the flow behavior over a rectangular wing in the subsonic wind tunnel in Iran was conducted. The tests included, surface pressure measurements at three locations and wake study at different angles of attack and free-stream Reynolds number. Further, to investigate the sidewall effects on the model pressure and wake, suction were applied at the wing root, where the model was attached to the tunnel wall. Suction affected surface pressure at all three locations by increasing the model pressure peak, preventing separation near the T. E., etc. at low angles of attack. However at moderate to high angles of attack, suction affected only the root pressure distribution.

1 Introduction

The wind is a free, clean, and inexhaustible energy source. Generating electricity from the wind is a mature technology and economically competitive with most fossil fuel applications, depending on the location. Wind turbines offer an attractive energy option for tourism businesses situated in coastal areas, flat open plains and mountain passes exposed to the consistent winds. Blades are where the turbine meets the wind. Turbine blades take advantage of aerodynamics to extract the wind's energy, which can then be converted to useful electricity. Airfoils determine the aerodynamic forces on the blade. They are key to the blade design. The design and performance assessment of wind turbines is presently performed almost always by means of blade element theories. A method based on the Blade Element Momentum for calculating the performance; hence power output of wind turbine blades including viscosity effects is being developed at the Aerospace Engineering Department of Sharif University. In order to provide experimental data for proper mathematical modeling as well as for testing the validity of the calculation a series of experiments have been conducted in a 0.8m x 0.8m low speed wind tunnel. The model was a rectangular wing where its cross section is an airfoil used in a 660 KW wind turbine blade. To author's knowledge, no experimental or theoretical results concerning the performance of the blade or the aerodynamic characteristics of the airfoil used in it are available. To achieve higher Reynolds number and to place more pressure tubes inside the model, the wing was tested as a half model. The half model technique is often used in aerodynamic testing but one must be careful with the secondary flow developments and its characteristics where the model is attached to the wall. A qualitative three-dimensional separations phenomenon for a flat-plate flow against a cylindrical obstacle that causes such a secondary flow is shown in figure 1. Further, to investigate the secondary flow effects on the model pressure and wake which is affected by the sidewall boundary layer and its separation near the wing junction, suction were applied on the wind tunnel sidewall, where the model was attached to it.

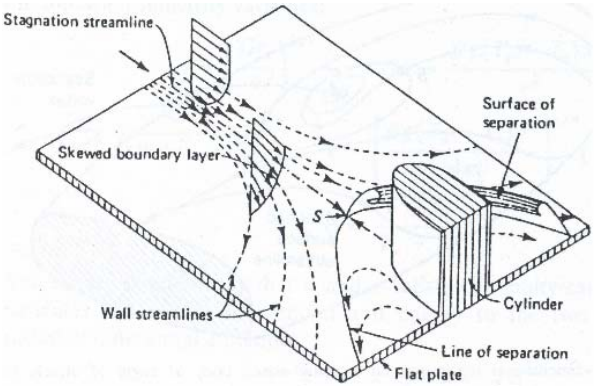

Fig. 1. Three-dimensional separation in flat-plate flow against a cylindrical obstacle [1].

2 Experimental Setup

The subsonic close circuit wind tunnel shown in figure 2 has a rectangular test section and operates at speeds from 10 to 100 m/sec. continuously. The wing had a span of 0.6 m and a uniform chord of 0.25 m and was mounted at its root on the wind tunnel sidewall center. The wing section was equipped with 29 pressure ports of 0.8 mm inner diameter at three different span location, $\frac{y}{b}$ = .067, 0.5 and 0.95. Figure 3 shows the wing section shape and the location of the pressure ports on it at each three locations. The tests were conducted at angles of attack ranging from -5 to 25 deg. and at three free-stream velocities of 30, 60, and 80 m/s corresponding to the Reynolds numbers of 0.5×10^6, 1×10^6, 1.3×10^6 based on the chord of the wing. The data was acquired by a PC computer equipped with an analog to digital board as shown in figure 4.

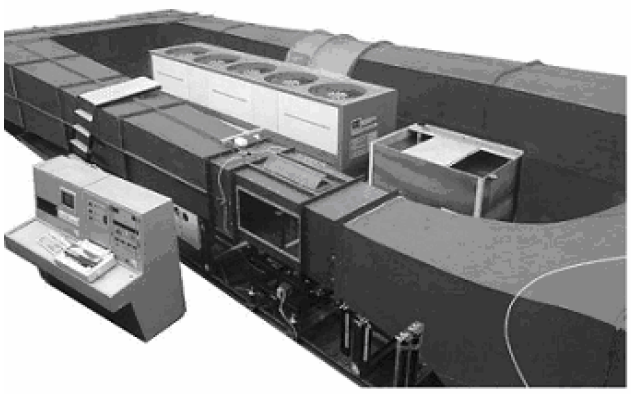

Fig. 2. Schematic of the wind tunnel.

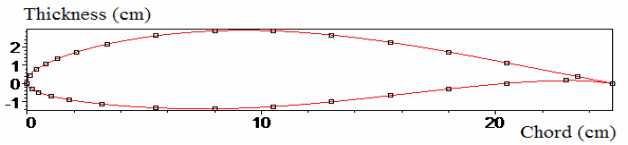

Fig. 3. Pressure port distribution on the model.

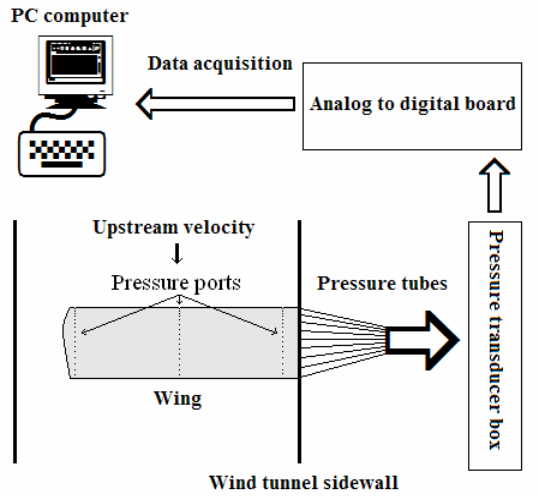

Fig. 4. Schematic diagram of the data acquisition system.

To study the wake behind both the model and wind tunnel sidewall boundary layer at various conditions, two rakes were designed and manufactured. The wake rake consisted of 67 total pressure probes and five static tubes along the 0.3 m vertical span. The boundary layer rake consisted of 32 total pressure probes and 1 static tube along the 0.075 m vertical span.
Measurements were conducted in two parts:

- Sidewall boundary layer profile for the empty tunnel with and without the suction.
- Half-model surface pressure, along with its wake at different angles of attack with and without suction.

3 Results and Discussion

As mentioned before, our first task was to study the performance of the newly designed suction mechanism. Hence, the sidewall boundary layer where the model is supposed to be installed was

studied at different free stream vehicles, V_∞=30, 60, and 80 m/sec. The experiments were conducted for both cases of suction on and off situation with and without the presence of the model. Figure 5 shows the velocity profile for the aforementioned cases for different free stream vehicles. From this figure, it is clearly seen that the sidewall boundary layer thickness increases as the free stream velocity increases, hence more suction is needed to diminish it totally. Furthermore, suction decreases the boundary layer thickness for all velocities considerably, however due to the limited suction rate, we were unable to draw in the entire boundary layer thickness as we expected.

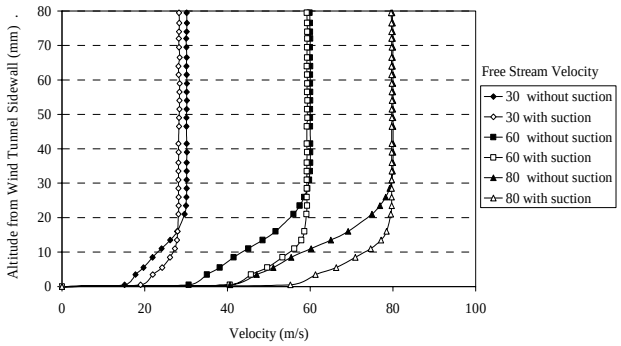

Fig. 5. Suction affects on sidewall boundary layer at three various free-stream velocities without model.

At the second step, the half-model surface static pressure and wake with and without suction were measured. Aerodynamic characteristics such as lift, pressure drag and total drag coefficient are calculated from the acquired data [2]. Figure 6 compares the lift coefficient variation versus angle of attack at the wing center line section and at the section located at $\frac{y}{b}$ = .067. The data are also compared with those obtained for the similar model, but in a 2-D test case. From this figure, it is clearly seen that sidewall effects cause a sharp decrease of lift coefficient near the root section as compared with wing mid section and the 2-d cases. As seen from this figure the calculated lift coefficient for both the mid section and the one near the wall are much less than the corresponding value for the 2-D case. The lift curve slope in the linear range of C_l vs α curve for the 2-D case is much higher than those of the 3-D ones and the lift behavior beyond the stall differs from each other too.

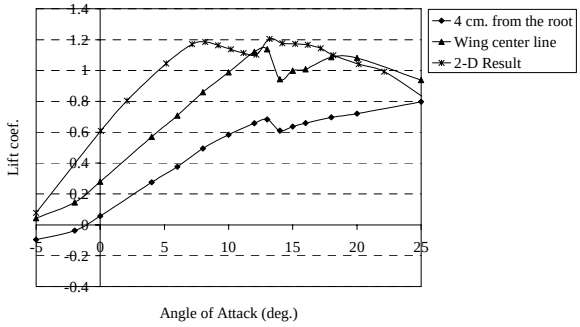

Fig. 6. Lift coefficient versus angle of attack near the wing root, at center line (Re=1.0*10^6).

Figures 7 to 16 show static pressure distribution of the model for suction close to the tunnel wall, $\frac{y}{b}$ = .067. The data are presented for two different Reynolds number and for ranges of angles of attack, α = -5 to 14 degrees for both suction on and off cases. From these figures it is clearly seen that for all angles of attack, the flow over a large portion of the model for the suction off case is separated. For example at α = 0 deg. , figure 12 shows that for the suction off case, the upper surface pressure coefficient, C_{p_u} , is nearly constant for $\frac{x}{c}$ > 0.6, while the 2-D data depicted on the same figure, does not show any sign of separation for this angle of attack. Similar situation is seen for 10 degrees angle of attack, Fig.13. , where C_p for the upper surface is nearly constant for $\frac{x}{c}$ > 0.3 for the suction off case. However, for 2-d data shown on the same figure C_p varies from the leading edge to the trailing edge, Fig.13. This early separation phenomenon seen for this portion of the model is probably caused by the interaction of the tunnel boundary layer with

that of the model one, hence enhancing flow separation in this region. The adverse pressure gradient caused by the model flow field affects the tunnel boundary layer and promotes early separation. This separated flow which looks like horseshoe vortex generates span wise velocity along with an adverse pressure gradient field along the model, thus separating the flow in the trailing edge region at all angles of attack. However, when the suction is applied at a rate about 1200 m^3/hr, the boundary layer thickness along the tunnel wall reduces significantly, Fig.5, thus the flow separation over the model delays to higher angles of attack.

This phenomenon is clearly seen by examining figures 7 thru 16 where for the suction on cases, C_p distribution along the chord has been smoothened and flow separation is delayed significantly. Furthermore, from these figures it is seen that the effect of suction on the pressure distribution for Re=$0.5*10^6$ is more pronounced than that of Re= $1*10^6$ case. For both Reynolds number tested, suction influences the pressure distribution in the adverse pressure gradient portion of the model more than that of the favorable portion, leading edge, one. In addition, as alpha increases, the effect of suction on the pressure distribution decreases, Fig.13-16.

Figures 17 and 18 show pressure distribution for two different Reynolds number measured at the wing centerline: $\frac{y}{b}$ =1/2, at an angle of attack of 10 degrees. Pressure data for 2-D model is also provided on the same figure for comparison. From Fig.17, it is clearly seen that for Re=$0.5*10^6$ case, static pressure distribution for this wing is almost exactly equal to that of 2-D one when the suction is on. However, for the suction off case, significant differences for the upper surfaces distribution is seen, Fig. 17. This comparison implies that the suction mechanism with the aforementioned rate is suitable for the low Reynolds number ones. As Reynolds number is increased to Re=$1*10^6$, 2-d data and the present data do not match, Fig.18. It is seen from this figure, Fig.18, that for this Reynolds number, suction does not change surface distribution significantly, hence it seems that the suction rate must be increased.

Effects of suction and Reynolds number on the surface pressure ports located near the wing tip, $\frac{y}{b}$ =0.95, are shown in Figs. 19 and 20 for 10 degrees angles of attack. These figures clearly show that boundary layer suction does not effect the pressure distribution for this portion of the wing significantly and the small effects are mainly concentrated near the wing leading edge, Figs. 19 and 20. For pressure ports located at $\frac{x}{c} > 0.5$ for the Re=$0.5*10^6$ and for ports located at $\frac{x}{c} > 0.3$ for the Re=10^6 cases, suction has no effect as seen from these figures.

Figures 21 and 22 illustrate dynamic pressure loss behind the model at various stations for 2 different angles of attack and for a constant Reynolds number of $1*10^6$ without suction. These figures clearly show the effect of wall boundary on the dynamic pressure distribution and the loss for the $\frac{y}{b}$ = .142 case is much more than the other cases, Figs 21 and 22. Furthermore, by the inspecting these figures, it is seen that the effect of angle of attack on the station located between $0.75 \le \frac{y}{b} \le 0.42$ is minimal, while for stations $\frac{y}{b}$ = .25 and .142, the effect is significant.

Effect of wall boundary layer suction on the dynamic pressure loss behind the model at two different station, $\frac{y}{b}$ = .142 and $\frac{y}{b}$ = .25, for various angles of attack and for a constant Reynolds number of Re= $1*10^6$ are shown in figures 23 and 24. Data for the suction off cases are also shown for comparison. As seen from these figures, suction reduces the dynamic pressure loss and decreases the width of the wake, hence causing a reduction in the drag force that is calculated by the momentum deficit method, as shown in Fig. 25.

\

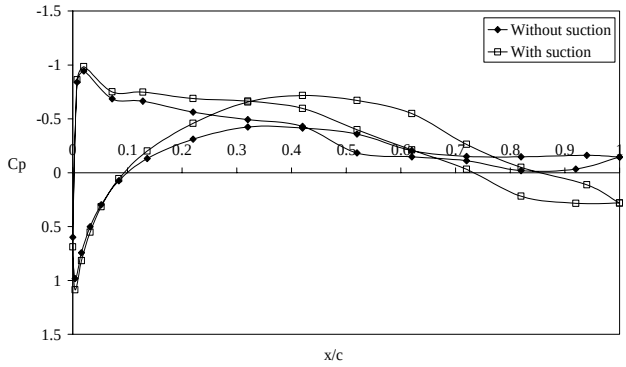

Fig. 7. Pressure coefficient for α = -5 deg. at $\frac{y}{b}$ = .067 (Re=0.5*10^6).

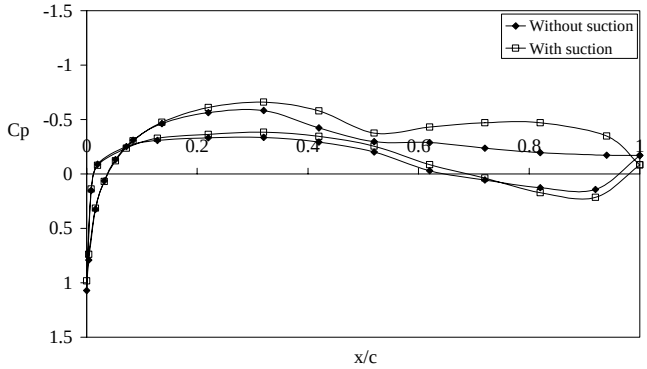

Fig. 10. Pressure coefficient for α = 0 deg. at $\frac{y}{b}$ = .067 (Re=1.0*10^6).

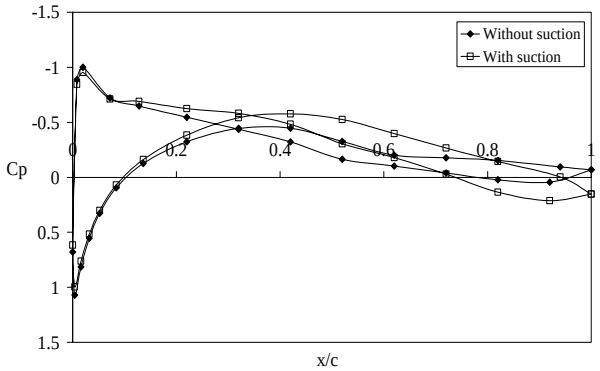

Fig. 8. Pressure coefficient for α = -5 deg. at $\frac{y}{b}$ = .067 (Re=1.0*10^6).

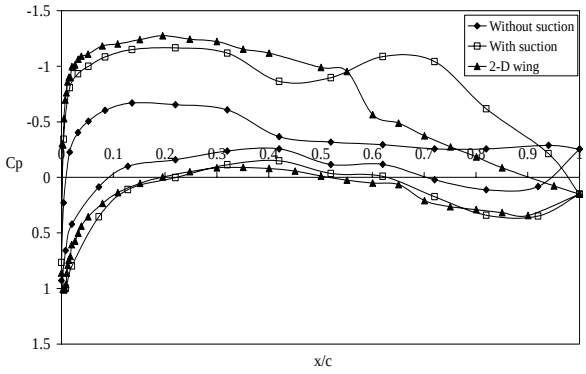

Fig. 11. Pressure coefficient for α = 4 deg. at $\frac{y}{b}$ = .067 (Re=0.5*10^6).

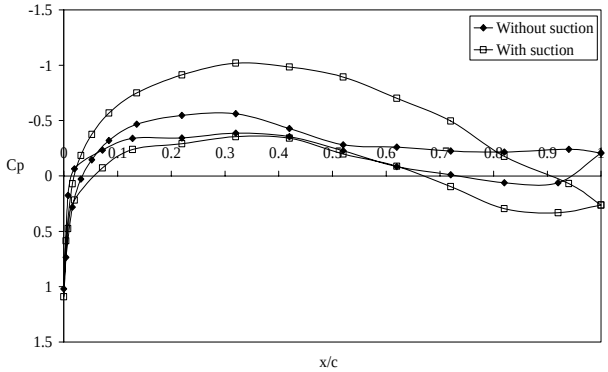

Fig. 9. Pressure coefficient for α = 0 deg. at $\frac{y}{b}$ = .067 (Re=0.5*10^6).

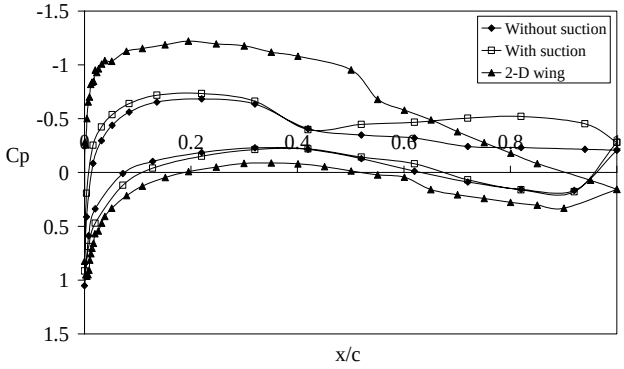

Fig. 12. Pressure coefficient for α = 4 deg. at $\frac{y}{b}$ = .067 (Re=1.0*10^6).

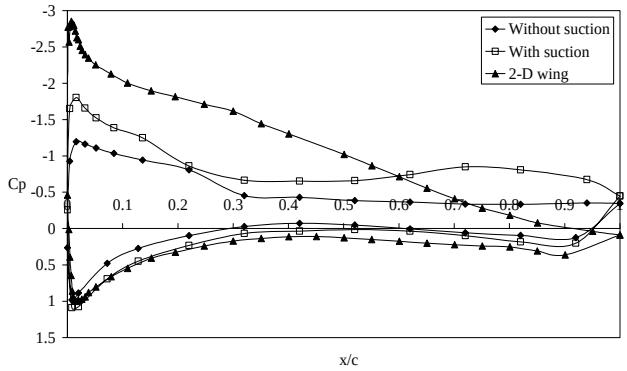

Fig. 13. Pressure coefficient for α = 10 deg. at $\frac{y}{b}$ = .067 (Re=0.5*10^6).

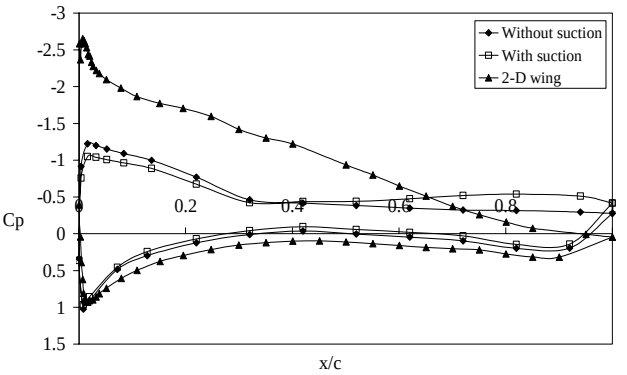

Fig. 14. Pressure coefficient for α = 10 deg. at $\frac{y}{b}$ = .067 (Re=1.0*10^6).

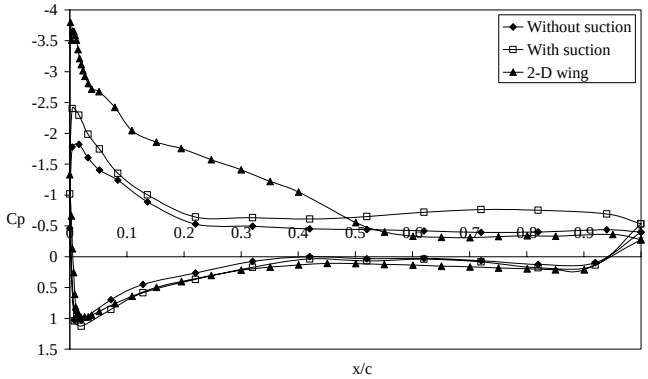

Fig. 15. Pressure coefficient for α = 14 deg. at $\frac{y}{b}$ = .067 (Re=0.5*10^6).

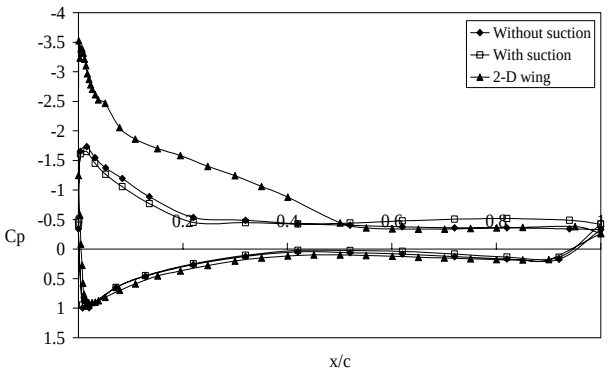

Fig. 16. Pressure coefficient for α = 14 deg. at $\frac{y}{b}$ = .067 (Re=1.0*10^6).

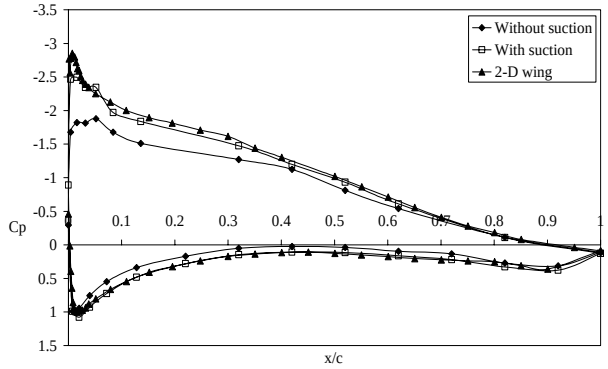

Fig. 17. Pressure coefficient for α =10 deg. at $\frac{y}{b}$ = .5 (Re=0.5*10^6).

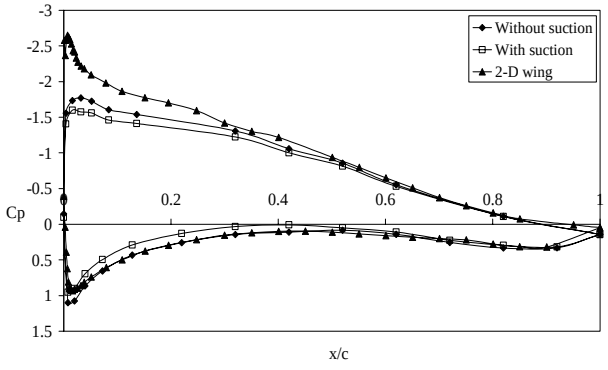

Fig. 18. Pressure coefficient for α = 10 deg. at $\frac{y}{b}$ = .5 (Re=1.0*10^6).

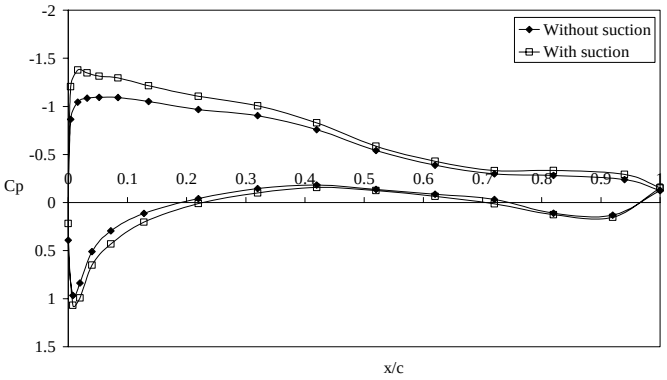

Fig. 19. Pressure coefficient for α = 10 deg. at $\frac{y}{b}$ = .95 (Re=0.5*10^6).

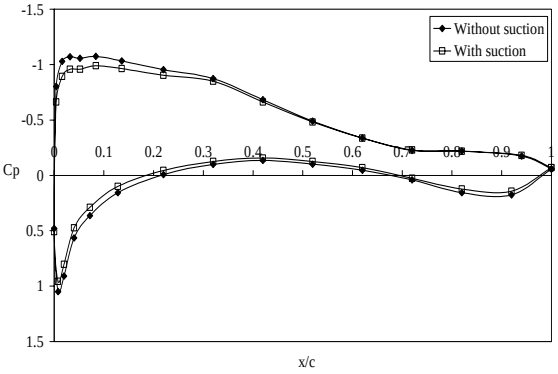

Fig. 20. Pressure coefficient for α = 10 deg. at $\frac{y}{b}$ = .95 (Re=1.0*10^6).

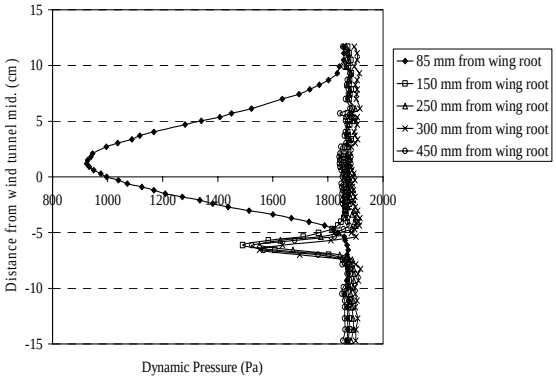

Fig. 21. Wake distribution across the wing span for α = 4 deg. (Re=1.0*10^6).

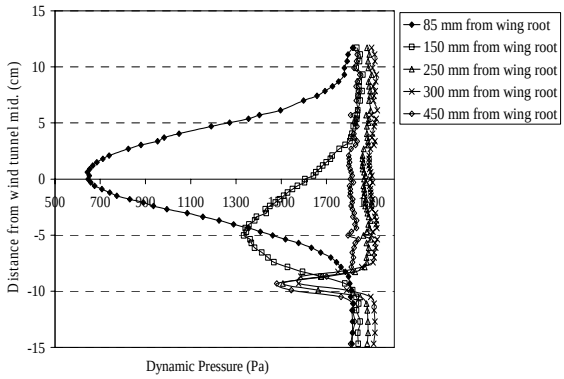

Fig. 22. Wake distribution across the wing span for α = 10 deg. (Re=1.0*10^6).

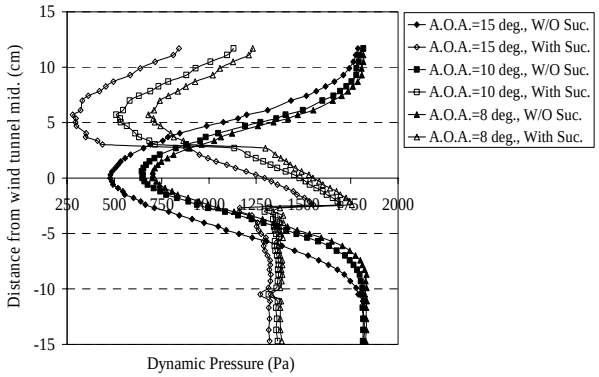

Fig. 23. Suction effect on wake at $\frac{y}{b}$=.142 (Re=1.0*10^6).

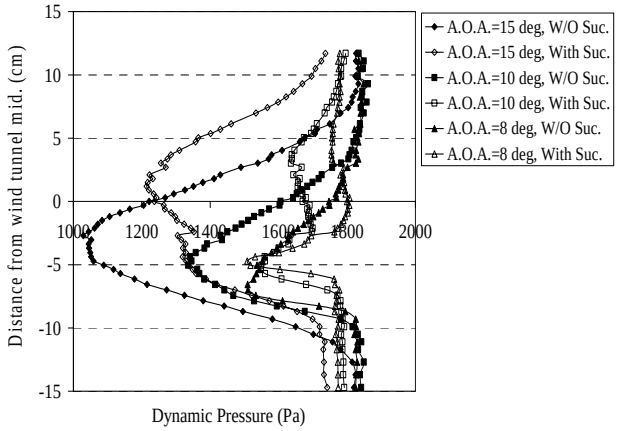

Fig. 24. Suction effect on wake at $\frac{y}{b}$=.25 (Re=1.0*10^6).

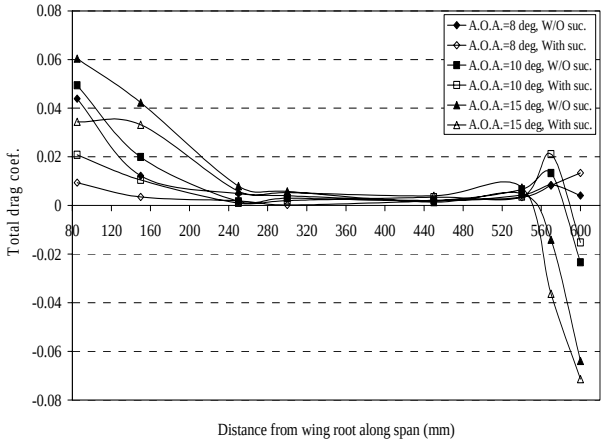

Fig. 25. Suction effect on the drag coefficient (Re=1.0*10^6).

4 Conclusions

A series of low speed wind tunnel tests on a rectangular wing were conducted to investigate the flow field and the corresponding pressure distribution along its span at various conditions. Prior to conducting 3-D experiments, various 2-D tests on similar airfoil which is used in a wind turbine blade were performed and the data are used to analyze the blade aerodynamic behavior, hence its performance criterion. The data clearly show that the pressure varies along the span of the model and it is seen that wing stall happens first at the root where the flow is seen to be separated up to about 70 % of the chord. Suction has significant effect on the pressure distribution mainly around the wing root. Our results show that the flow over the portion of the model effected by the sidewall boundary layer separates at angle of attack which is smaller than the corresponding angle for other portions of the wing. This phenomenon yields an increase in the drag coefficient and a sharp decrease in the value of the lift coefficient. However, when suction was applied to the sidewall, separation was delayed to higher angles, and the corresponding aerodynamic loads varied significantly.

Acknowledgements

This work has been carried out at the Department of Aerospace Engineering at Sharif University of Technology. The financial support provided by the Iranian NEDC is gratefully acknowledged.

References

[1] Frank M. White**.** *Viscous fluid flow*. 2nd edition, McGraw-Hill, Inc., 1991.

[2] Rae, H. W., Jr. & Pope, A. *Low-speed wind tunnel testing*. 3rd edition, John Wiley & Sons, Inc.,1999.

[3] Soltani M. R., Askary seydshokri F. and bakhshalipour Kalkhoran A. B. Roughness and turbulence effects on the aerodynamic efficiency of a wind turbine blade section. *International Aerospace Conference*, Ankara, AIAC-2005-057.